Numerical analysis of co-flowing immiscible liquids in co-axial microtubes: flow regimes map and boundaries correlations

In-Hwan Yang[1,2] and Mohamed S. El-Genk[1,2,*]
[1]Institute for Space & Nuclear Power Studies,
[2]Chemical & Nuclear Engineering Dept. and 3Mechanical Engineering Dept.
University of New Mexico, Albuquerque, NM, USA

Abstract

Performed numerical analysis of co-flowing immiscible liquids in co-axial microtubes investigated the effects of changing the injection velocities and physical properties of the liquids, the interfacial tension and the diameters of the co-axial microtubes on forming disperse droplets in various regimes. The regimes are dripping, transition and jetting. Results, covering a wide range of parameters, identify the conditions for the common boundaries between these regimes. The developed dimensionless correlations, based on numerical results and generated motion picture movies of up to 18 cycles of forming the droplets, accurately predict theses boundaries. Favorable comparisons of present results with those of others and with reported experimental data validate the numerical methodology, the developed flow regimes map as well as the developed correlations for the boundaries between the various flow regimes. These correlations are in good agreement with the present numerical results to within ±10% and with the reported data of experiments used different immiscible liquids to within ±20%. These liquids include ionized water (disperse liquid) and PDMS (Polydimethylsiloxane) oil with $R^* = 10$, and aqueous solution of glycerine (disperse liquid) and silicone oil, with and without surfactant (Sodium Dodecyl Sulfate) and $R^* = 13.8$.

1. INTRODUCTION

The desire to produce monodisperse microemulsions on an industrial scale using microfluidic methods has stimulated numerous investigations, involving numerical simulations and small-scale experiments [1-12]. Of particular interest, is using co-flowing immiscible liquids in co-axial microtubes (Fig. 1) to produce microemulsions of monodisperse droplets. This method offers precise control of the size, formation frequency and monodispersity of the forming microdroplets. Owing to its simplicity and applicability to large scale production, this method is an effective alternative to injecting disperse liquid through an orifice into a stationary immiscible liquid, which is inefficient and produces highly polydisperse emulsions [13 - 15].

The production of monodisperse emulsions is highly desirable in many industries and biomedical applications. Examples are food processing, fertilizer, animals feed, chemical, petroleum, energy, pharmaceutical, cosmetics polymerization industries and water purification and desalination. In healthcare, micro-emulsions are used or being considered for advanced medical procedures, drug delivery, immunization, and microanalysis, just to mention a few.

There are three basic flow regimes for forming disperse droplets using co-flowing immiscible liquids in co-axial microtubes (Fig. 1) [5], namely: dripping, transition (or poly disperse dripping) and jetting. Shifting from one regime to the other occurs by changing the injection velocities and physical properties of the liquids, the interfacial tension and/or the diameters of the co-axial capillary tubes.

*Corresponding author: Regents' Professor and Director, Tel: (505) 277 – 5442, E-mail: mgenk@unm.edu

Such changes also affect the size and formation frequency of the disperse droplets [5], and the common boundaries between the various regimes. The latter is the focus of this paper.

The dripping regime at low injection velocities produces monodisperse droplets. The pinch-off and eventual breakup of the droplets are caused by the interfacial tension force near the exit of the disperse liquid capillary nozzle (Figs. 1 and 2a). When the diameter of the continuous liquid microtube is much larger than that of the disperse liquid, the forming droplets are perfectly spherical (Fig. 2a). The droplet radius decreases with increasing the injection rate of the continuous liquid [5].

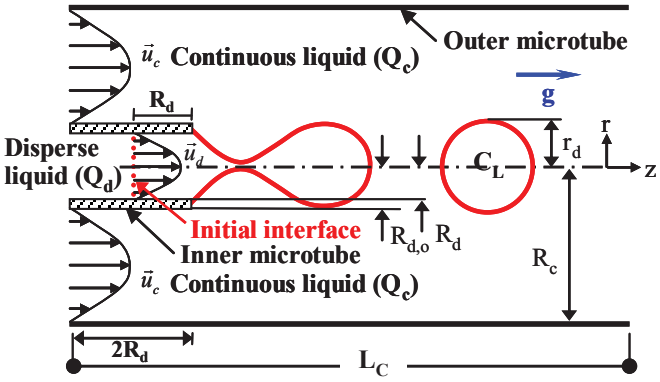

Figure 1. A Schematic of Disperse Droplets Formation in Dripping Regime using Co-Flowing Immiscible Liquids in Co-Axial Microtubes.

In the transition regime at higher injection velocities of immiscible liquids than in the dripping regime, a disperse-liquid thread forms. It extends from the exit of the disperse liquid nozzle to the growing "primary" droplet at the opposite end of the thread (Fig. 2b). The thread length could be as much as several droplet diameters. Following a pinch-off of the "primary" droplet by interfacial tension, the liquid thread separates from the disperse liquid nozzle and becomes hydro-dynamically unstable. It then breaks off into a number of "satellite" droplets of miniature sizes, by a combination of hydrodynamic instability and interfacial tension (Fig. 2b).

The average size of the primary droplets in the transition regime is typically smaller than in the dripping regime. The number and sizes of the forming satellite droplets depend on the injection velocities and physical properties of the co-flowing immiscible liquids. They also depend on the interfacial tension and the diameters of the coaxial microtubes [4,5]. Increasing the injection rate of the continuous liquid increases the length of the disperse liquid thread, decreasing the size of the primary droplet but increasing the number and sizes of the satellite droplets (Fig. 2b).

The shift from the transition to the jetting regime occurs when further increasing the injection velocities of the co-flowing immiscible liquids and/or decreasing the interfacial tension. These conditions increase the length of the disperse-liquid thread, which would not break off, but evolve into either a stable narrowing or widening jet (Fig. 2c). Disperse droplets break off at the tip of these jets by the combined effects of the viscous forces of the liquids (Fig. 1), interfacial tension and hydrodynamic instability [8-12]. The sequential break off of disperse droplets from the tip of jets is at a higher frequency than in the dripping and transition regimes. However, the size of the droplets depends on the type of the jet. A narrowing jet, with a decreasing diameter with distance from the tip of disperse-liquid microtube, produces relatively small, polydisperse droplets. A widening jet, with an increasing diameter with distance from the tip of disperse-liquid microtube (Fig. 2c), forms larger droplets and, sometimes, one or a few tiny satellite droplets. Identifying the condition leading to the formation of the two types of disperse liquid jets is a focus of this work. Table 1 summarizes the conditions and characteristics of forming disperse droplets in the different regimes discussed earlier and depicted in Fig. 2.

Recently, these authors [5] have numerically investigated the dripping and transition (or polydisperse dripping) regimes. Results were used to develop semi-empirical, dimensionless correlations for the radius and the formation frequency of disperse droplets. The correlations are formulated in terms of the continuous liquid capillary number and the ratios of Reynolds numbers and microtubes' radii of the co-flowing immiscible liquids, as:

$$r_d^* = 0.228\, R^{0.466} \left(\mathrm{Re}_d / \mathrm{Re}_c\right)^{0.5} / Ca_c^{-0.5} \tag{1}$$

$$f^* = 53.26\, Ca_c^{1.47} / \left\{ R^{1.369} \left(\mathrm{Re}_d / \mathrm{Re}_c\right)^{0.147} \right\} \tag{2}$$

These correlations applicable for $r_d < 0.5\, R_c$, are based on the results of numerical analysis for wide ranges of parameters. These are the injection velocities, microtube radii and physical properties of the co-flowing immiscible liquid as well as the interfacial tension. The correlations in Equations (1) and (2) are consistent with the reported numerical and experimental results by others [6,7]. They apply in the dripping regime (Fig. 2a) and also in the transition regime, but only when the total volume of the satellite droplets is < 1% of that of the primary droplets (Fig. 2b).

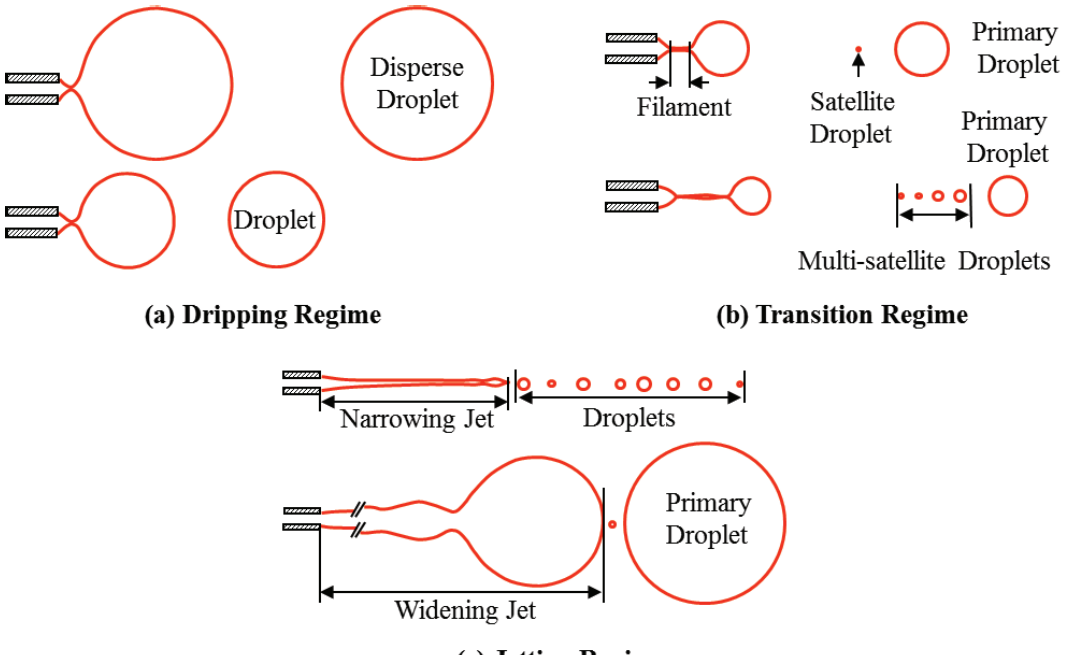

Figure 2. Illustrations of the Regimes for Forming Disperse Droplets Using Co-Flowing Immiscible Liquids in Co-Axial Microtubes.

Reported studies of co-flowing immiscible liquids in co-axial microtubes (Fig. 1) included both numerical and experimental investigations of the dripping and/or the jetting regime [3-6, 8-12]. Most considered the transition and dripping a single regime [3,4,6,8-12]. Thus, there is a need to parametrically investigate all three regimes of forming disperse droplets (Fig. 2), develop a regimes' map and identify the conditions for shifting from one regime to the other.

The objective of this work is to numerically investigate and characterize the flow regimes of forming disperse droplets using co-flowing immiscible liquids in coaxial microtubes (Figs. 1 and 2 and Table 1). A parametric analysis is conducted, which covers wide ranges of controlling parameters (Table 2). These are the injection rates and properties of the two immiscible liquids and the radii of the co-axial microtubes and the interfacial tension. The numerical results are used to develop a detailed flow regimes map and dimensionless correlations for the common boundaries among the various regimes. These are dripping, transition and jetting.

The numerical results are also used to generate motion picture moves to help characterize the formation dynamics of disperse droplets in the various regimes and the development of the regimes' map. Dimensionless correlations, based on the numerical results are developed for predicting the boundaries between the regimes of dripping, transition and jetting (Fig. 2). Numerical results and experimental measurements by others are used to validate the present calculations and confirm the fidelity of the numerical methodology and the developed flow regimes map and correlations for the boundaries between the regimes. The next section briefly reviews relevant literature and prior work.

Table 1. Regimes of Forming Disperse Droplets Using Co-Flowing Immiscible Liquids in Co-axial Microtubes.

Item	**Flow Regime**			
	Dripping	***Transition***	**Jetting**	
			Narrow	***Wide***
Condition	Moderate injection velocities, high interfacial tension, low viscous drag	Higher injection velocities and lower interfacial tension	High injection of continuous liquid and interfacial tension	Low injection of continuous liquid and interfacial tension
Emulsion	Mono-disperse droplets	Mono-disperse primary droplets, followed by tiny satellite droplets	Poly-disperse droplets of small sizes	Mostly mono-disperse large droplets with a few infrequent tiny satellite droplets
Primary droplets break off	Pinch-off by interfacial tension near the exit of disperse liquid microtube	Pinch-off by interfacial tension at far end of thin short disperse liquid thread	Hydrodynamic instability at far end of stable disperse liquid jets	
Satellite disperse droplets	Rare, depending on conditions	Form by breakup of disperse liquid thread by interfacial tension and instability	Infrequent, following break off of primary droplets	
Formation frequency of primary droplets	Lower than transition and narrow jetting, but higher than wide jetting	Higher than dripping and wide jetting, but lower than narrow jetting	Very high	Very low
Primary droplet size	Larger than in transition and narrow jetting, but lower than wide jetting	Much smaller than in dripping and wide jetting regimes	Smallest	Largest

2. A REVIEW OF RELEVENT LITERATURE

Limited experimental and numerical investigations have been carried out with co-flowing immiscible liquids in co-axial microtubes. A few attempted to develop a flow regimes map, with emphasis on the shift to the jetting regime. Cramer et al. [4], Utada et al. [8] Castro-Hernandez et al. [9], and Guillot et al. [10] have conducted experiments, which varied the interfacial tension and the injection velocities and dynamic viscosities of the c-flowing liquids to identify the condition for the shift to the jetting regime. Results did not specifically identify the transition regime (Fig. 2b); considering it a part of dripping, but identified the two distinct formations of disperse liquid jets: (a) *narrowing jets* and (b) *widening jets* (Fig. 2c). The narrowing jets form [8,9] when the injection velocity of the continuous liquid is much higher than that of disperse liquid. Conversely, the widening jets form when the injection rate of disperse liquid is much higher than that of the continuous liquid.

Experimental results of Cramer et al. [4] have shown that narrowing jets generally form at a relatively low disperse liquid velocity, when the viscosity ratio of the co-flowing liquids increases or the interfacial tension decreases. Their results also showed that increasing the disperse liquid velocity causes jetting to occur at a lower continuous liquid velocity. Cramer et al. [4] did not provide, however, a specific criterion for shifting to the jetting regime.

Utada et al. [8] and Castro-Hernandez et al. [9] have introduced a state diagram to characterize the conditions for shifting from dripping to jetting, assuming the transition regime is a part of dripping (Fig. 2). The diagram is based on the capillary number of the continuous liquid and Weber number of disperse liquid. When the effects of the viscous shear and inertia force of the liquids outweigh that of interfacial tension, disperse liquid jets form. Narrowing jets form when the effect of viscous shear of the continuous liquid outweighs that of interfacial tension. On the other hand, widening jets form when the viscous shear of disperse liquid increases and its inertia is negligibly small. Castro-Hernandez et al. [9] have conducted experiments, which investigated the criteria of Utada et al. [8] for the jetting regime. Results indicated that this regime occurs at a lower Weber number of the disperse liquid than indicated by Utada et al. [8].

In his investigations of the breakup of inviscid and viscous liquid jets, Rayleigh [16,17] assumed that an initially unperturbed surface of infinitely long jet could cause the jet to become unstable with time due to the growth of a linear perturbation. Tomotika [18] extended Rayleigh's instability to co-flowing immiscible liquids by considering the effect of continuous liquid viscosity.

Conlin and Tancogne [12] have investigated the conditions of shifting to the jetting regime for a system of co-flowing immiscible liquids. They calculated the maximum growth rate constant of the jet surface perturbation in terms of the wave number. They also proposed a critical length of disperse liquid jets (Fig. 2c), defined as the ratio of the maximum injection velocity and the maximum growth rate constant of the surface perturbations. They acknowledged the dripping and jetting regimes, based on the length of disperse liquid jets. They indicated that dripping occurs when the length of the disperse liquid thread is less than a critical length and the breakup of the droplets occurs by pinching off the liquid thread near the exit of the inner microtube (Fig. 1). Conversely, they considered the jetting region to occur when the length of disperse liquid thread equals or exceeds a critical length and the break off of disperse droplets occurs by surface instability at the far end of disperse liquid jet. Although Conlin and Tancogne [12] did not explicitly propose a value or an expression for the thread critical length for forming disperse liquid jets, they attempted that from the experimental results of Guillot et al. [10].

Based on the values of viscous shear and the inertial forces of the co-flowing immiscible liquids, Guillot et al. [10] have introduced the terms "*convective*" and "*absolute*" instabilities to distinguish dripping and jetting. They indicated that absolute instability occurs when the interface disturbances grow and propagate upstream, eventually pinching off the disperse droplets at or close to the exit of the inner microtube (Fig. 1). The transition to convective instability occurs, when the interfacial tension decreases and/or the injection velocities of the co-flowing liquids increase. With convective instability, growing perturbations propagate preferentially downstream, eventually pinching off the disperse droplets at the far end of a long disperse liquid thread or "jet".

Linear instability analysis of Guillot et al [10] radially averages the flows and the perturbations of

the co-flowing liquids and neglects their inertia. While the results of the analysis generally agree with their own experimental results, there were substantial deviations. Their experiments employed disperse aqueous solution of 50wt% glycerin and silicon oil. These liquids have viscosities of 55 mPa.s and 235 mPa.s. The radii of the capillaries for injecting the continuous and disperse liquids varied from 20-50 µm and 200-500 µm, respectively.

Herrada et al [11] have developed an axisymmetric instability model, similar to that of Guillot et al [10], but accounted for the inertia of disperse and continuous liquids. Herrada et al [11] considered perturbed, 3-D liquids flows and compared the results of their instability analysis with their own experimental results and those of Guillot et al [19]. In their experiments, Herrada et al. [11] varied the diameter of the disperse liquid microtube from 40-100 µm and that of the continuous liquid micotube was either 550 or 860 µm. Their experiments used three pairs of disperse and continuous liquids (water with a viscosity of 1.0 mPa.s and hexadecane with a viscosity of 3 mPa.s, water-glycerin solution with a viscosity of 55 and silicone oil with a viscosity of 235 mPa.s, and water-glycerin solution with a viscosity 650 mPa.s and silicone oil with a viscosity of 235 mPa.s). They controlled the interfacial tension in the experiments by adding sodium dodecyl sulfate to the aqueous solutions and Span-80 to the hexadecane.

The hydrodynamic instability analysis is useful for characterizing the jetting regime [10-12,16-26]. However, it does not acknowledge the transition regime, between dripping and jetting. To the best knowledge of these authors, no distinct criteria have been proposed for determining the three regimes, discussed earlier and depicted in Fig. 2, of forming disperse droplets. This need is addressed in the present work.

For clarity, these authors define dripping as the regime for producing monodisperse droplets, which break off at the exit of the inner capillary (Fig. 1) by interfacial tension (Fig. 2a). For both widening and narrowing stable jets, disperse droplets break off by hydrodynamic instability at the far end of the jets (Fig. 2c). In the transition regime, between dripping and jetting, the break off of the primary disperse droplets at the far end of a short liquid thread is mostly by interfacial tension. In this regime, the break off of the primary droplet is followed by the formation of a number of tiny satellite droplets (Fig. 2b).

The next section reviews the governing equations used in the present numerical analysis for simulating co-flowing immiscible liquids in co-axial microtubes and identifying the conditions of the boundaries between dripping, transition and jetting regimes (Fig. 1).

3. GOVERNING EQUATIONS

The present numerical analysis tracks the evolving interface between the co-flowing immiscible liquids and solves the transient momentum and continuity equations of the liquids, subject to the momentum jump condition at the interface. It assumes non-slip at the walls of the co-axial microtubes. The interface evolves under the effects of interfacial tension, inertia and viscous drag forces of the co-flowing liquids (Fig. 1). The location and shape of the evolving interface between the liquids (Fig. 3) are determined in the numerical solution using the Level Set method [5,27,28]. The commercial software package of COMSOL 4.0a is used to solve the governing equations and implement the Level Set method [28].

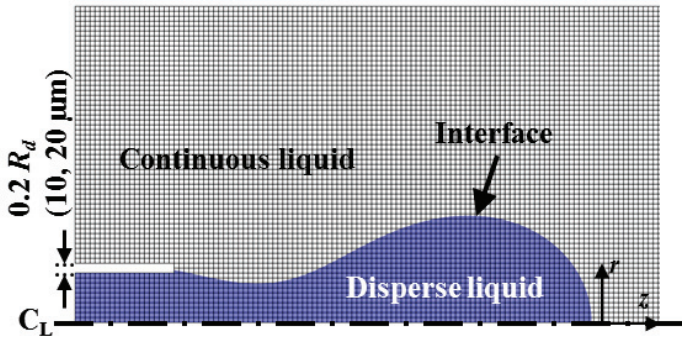

Figure 3. Numerical Grid Implemented in the Present Numerical Simulations.

Details of the governing equations, initial and boundary conditions and the modeling approach can be found in [5], and are only summarized herein. The continuity and momentum balance equations of the co-flowing, incompressible, Newtonian immiscible liquids are given as:

(a) Continuity:

$$\frac{\partial \rho_n}{\partial t} + \rho_n \nabla \cdot \vec{u}_n = 0 \tag{3}$$

(b) Momentum balance:

$$\rho_n \frac{\partial u_n}{\partial t} + \rho_c u_n \cdot \nabla u_n = -\nabla p + \mu_n \nabla^2 u_n + \rho_n g + F\delta \tag{4}$$

In equation (4), the interfacial force, F, acting normal onto the interface (Fig. 3) is determined in terms of the difference in the normal stresses exerted onto the interface by the hydrodynamic forces of the co-flowing liquids and that associated with the local curvature of the interface, κ, and the interfacial tension coefficient, $\sigma_{d,c}$ [5]. Within the computational domain (Fig. 3) the interfacial force, F, is valid only at the interface. A function, δ, is introduced in the momentum balance, equation (4), to account for the momentum jump at the interface between the co-flowing liquids in the numerical solution. This function is unity at the interface and zero elsewhere in the computation domain [5,28], thus:

$$F = \sigma_{d,c} \vec{n} \kappa = \vec{n} \left(\tau_c - \tau_d \right) \tag{5}$$

The location of the interface is determined from the solution of the following advection equation:

$$\frac{\partial \varphi}{\partial t} + u_{\text{int}} \cdot \nabla \varphi = 0 \tag{6}$$

In this equation, $\phi(r, z)$ is a scalar function that indicates the location of the evolving interface between the co-flowing liquids in the computation domain [5,28] (Fig. 3). The present analysis neglects the viscous heat dissipation in the momentum equations, owing to the very low injection velocities of the two immiscible liquids [29]. It is for disperse droplets diameters less than the inner diameter of the continuous liquid microtube (Fig. 1).

In the analysis, the co-flowing liquids are injected continuously at constant volumetric flow rates, or average velocities, into co-axial microtubes (Fig. 1). The gravitational force, g, aligned with the centerline, C_L, of the co-axial microtubes, does not affect the flow dynamics of the liquids. The analysis also assumes axisymmetric, isothermal fully developed laminar flows. At the start of the numerical simulation, $t = 0$, the inner microtube is assumed filled half way (or $z = R_d$) with disperse liquid, while the continuous liquid fills the rest of the computational domain (Fig. 1). The solution of Equations (3) and (4), with the advection equation (6), tracks the movement and evolution of the interface, initially located a distance R_d from the tip of the disperse-liquid microtube (Fig. 1) [5].

Table 2. Ranges of Properties and Parameters Investigated.

Parameter	Base Values	Range in Analysis	Units	Parameter	Base Values	Range in Analysis	Units
R_d	50	50 – 100	μm	Q_c	9.622	0.1924 – 9900	μl/s
R_c	320	160 – 2020	μm	$\bar{u}_c$	0.031	0.00037 – 2.48	m/s
μ_d	0.031	0.0031 – 0.124	Pa·s	R^*	6.4	3.2 – 20.2	–
μ_c	0.031	0.0031 – 0.124	Pa·s	Re_d	0.1	0.02 - 1	–
ρ_d	1000	1000	kg/m^3	Re_c	0.52	0.0033 – 74.4837	
ρ_c	1000	1000	kg/m^3	Ca_d	0.0481	0.0016 – 0.3844	–
$\sigma_{d,c}$	0.02	0.01 - 0.0961	N/m	Ca_c	0.0481	0.0003 – 0.55	–
Q_d	0.243	0.0487 – 2.4357	μl/s	We_d	0.00481	0.0002 – 0.1602	
$\bar{u}_d$	0.031	0.0062 – 0.31	m/s	Re_d/Re_d	0.1923	0.0003 – 153.846	–

Figure 3 shows the numerical mesh grid used in the computation domain of the present numerical simulations. The domain comprises quadrilateral mesh elements of a uniform size (5 x 5 μm). However, the total number of the mesh elements increases from 9,560 to 60,650, commensurate with the radius of the continuous liquid microtube (Table 2). The computation domain in the present simulations, from the tip of the disperse liquid capillary, is long enough to obverse at least 3-5 cycles, and in some cases up to 18 cycles, of forming disperse droplets (Fig. 2), depending on the prevailing regime (dripping, transition or jetting).

Using a finer numerical grid, insignificantly changes the numerical results, including the diameter and formation frequency and the prevailing regime of forming disperse droplets, but increases the computation time [5]. The numerical solution fully converges with < 6% error in the overall mass balance of the disperse liquid. This error is mostly due to the formation of very tiny satellite droplets in the computation domain that are difficult to account for in the overall mass balance.

The numerical simulations are performed on a cluster of 8-quad core processors (2.27 GHz Xeon) and 120 GB of memory. The computation time for each simulation varied from 72 to 168 hours of real time. Table 2 lists the values of the base case parameters (2nd and 6th columns), and their ranges used in the simulations (3rd and 7th columns). The next section presents the results of the performed parametric numerical analysis for the range of parameters listed in Table 2.

4. RESULTS

The objectives of the present numerical simulations include developing a flow regimes map and determining the conditions for the boundaries between the dripping, transition and jetting regimes. Results are used to produce motion picture movies to help characterize the dynamics of the formation, growth and break off of disperse liquid droplets in the dripping, transition and jetting regimes (Fig. 2). In addition to the volume of the droplets, their formation frequencies are also determined.

4.1 Volume and Frequency of Disperse Droplets

Figure 4-7 plot the calculated volumes of the primary and satellite disperse droplets and the frequency of forming the primary droplets in the dripping, transition, and jetting (narrowing and widening jets) regimes. The values of the parameters used in the numerical simulations to generate the results in these figures are: R_d = 50 μm, R_c = 320 μm (or R^* = 6.4), $\bar{u}_d$ = 0.031 m/s, $\bar{u}_c$ = 0.0248 m/s, μ_d and μ_c = 0.031 Pa·s, ρ_d and ρ_c = 1000 kg/m^3, and $\sigma_{d,c}$.= 0.03 N/m.

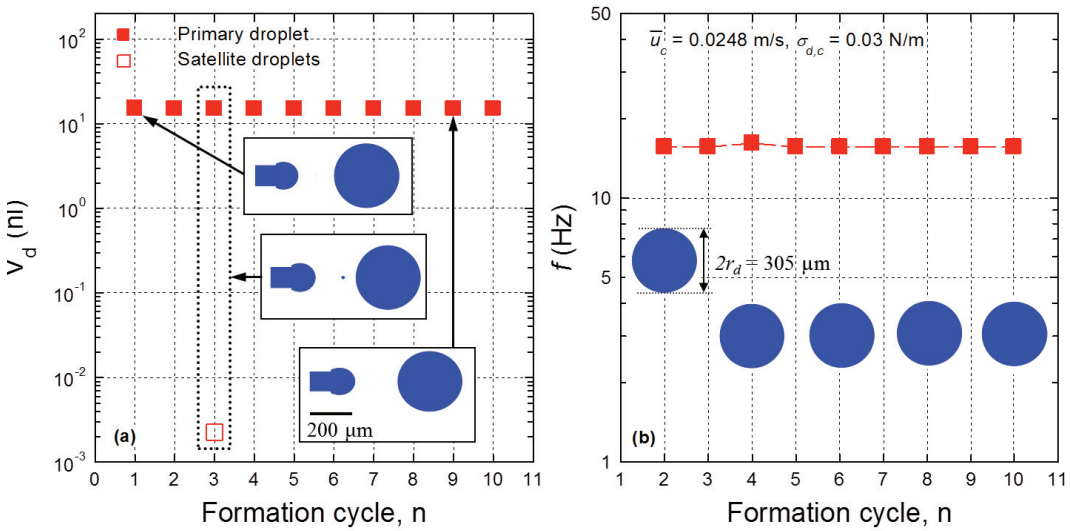

Figure 4. Changes in Disperse Droplet Volume (a) and Formation Frequency (b) in Dripping Regime.

Results presented in Figures 4a and 4b are for the dripping regime. The disperse droplets have exactly the same size (or radius), irrespective of the formation cycle. They are perfectly spherical with an identical volume of 15.1 nl and a radius, r_d, of 152.5 μm (Fig. 4a). The droplets are monodisperse, despite the formation of a single tiny satellite droplet in a few of the simulations. For all forming disperse droplets in the dripping regime, excluding the first, the formation frequency is constant 15.6Hz (Fig 4b).

Increasing the injection velocity of the continuous liquid, $\overline{u}_c$, from 0.0248 to 0.1085 m/s, while keeping all other parameters in Table 2 constant, shifts the formation of the disperse droplets from the dripping to the transition regime (Figs. 5a and 5b). In this regime, the interfacial shear exerted by the high injection rate of the continuous liquid develops a short thin filament or *"thread"* of disperse liquid. It extends from the exit of the inner microtube to the evolving primary droplet at the opposite end (Fig. 2b). The disperse droplets break off by necking the filament under the effect of interfacial tension. Following the primary droplet's pinch off, the thin disperse liquid filament breaks off at the exit of the inner microtube and becomes hyrodynamically unstable. It breaks down into one or more tiny satellite droplets, under the combined effects of the interfacial tension and hydrodynamic perturbations at the the surface of the filament. The total volume of the forming satellite droplet is negligibly small (< 2.5% of the primary droplet) (Fig 5a).

In the transition regime, the formation of a primary disperse droplet is associated with a couple of satellite droplets of different, but very small volumes (Fig. 5a). The primary droplets are perfectly spherical, but of much smaller volume than in the dripping regime (Fig. 4a). The primary droplet in Fig. 5a is 1.57 nl in volume and has a radius, r_d = 72.5 μm. The average formation frequency of the primary droplet in Fig. 5b is 147.1 Hz, excluding the first droplet. This frequency is almost an order of magnitude higher than that in the dripping regime of 15.6 Hz (Fig. 4b). It is worth noting that the inconsistent sizes of the satellite droplets in the transition regime slightly affect the formation frequency of the primary droplets. This frequency in the 2nd to 10th cycle fluctuates between 144.9 and 151.5 Hz (within 1.5 to 3 % of the average frequency) (Fig. 5b).

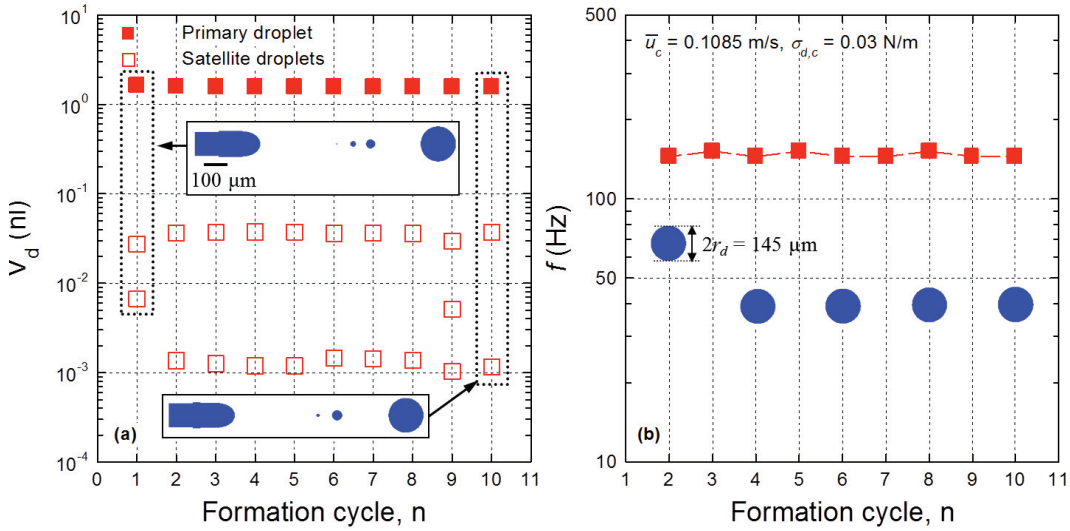

Figure 5. Changes in Disperse Droplet Volume (a) and Formation Frequency (b) in the Transition Regime.

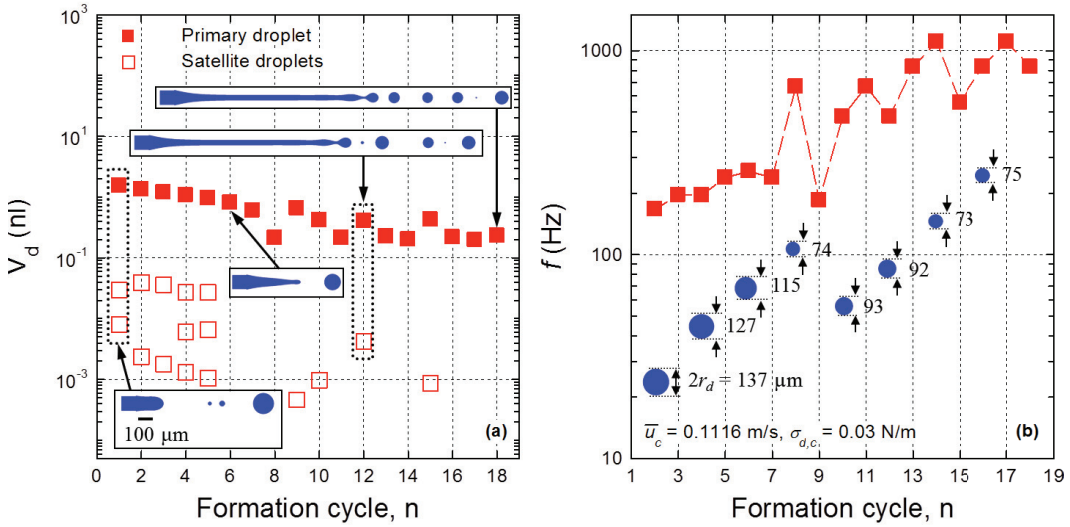

Figure 6. Changes in Disperse Droplet Volume (a) and Formation Frequency (b) with a Narrowing Jet.

Increasing the injection velocity of continuous liquid, $\overline{u}_c$ to 0.1116 m/s, while keeping all other parameters in Table 2 constant, shifts the formation of disperse droplets to the jetting regime (Figs. 6a and 6b). In this regime, polydisperse droplets break off at the tip of a stable disperse liquid jet by the hydrodynamic instability and the propagation of the growing surface perturbations along the jet. The narrowing jet in Fig. 6a produces droplets of inconsistent volumes with inconsistent frequencies.

The volumes of the droplets generated by narrowing jets (Fig. 6a) are much smaller and the corresponding frequencies are much higher than in the transition regime. The inserted images in Fig. 6a show that a stable disperse liquid jet does not form until the 6th cycle of the simulated transient, and its length increases thereafter. By the 18th cycle, the length of the stable narrowing jet reaches ~1540 μm

(Fig. 6b). In the first 5 cycles, the volume of the produced disperse droplets, before establishing a stable narrowing jet, decreases and the formation frequency increases graduating with the number of cycles.

After the formation of a stable narrowing jet (n ≥ 6) the average volume of disperse droplets continues to decrease at an increasing frequency (Figs. 6a and 6b). As these figures show, disperse droplet produced by a narrowing jet are highly polydisperse. During the simulated cycles 6-18, the average volume of the disperse droplets oscillates between 0.198 to 0.806 nl, with a average radius of ~ 14 to 58 µm. The average formation frequency of the droplets in the last 13 cycles is 634.1 Hz, oscillating but steadily increasing from ~ 200 Hz in the 6th cycle to over 1000 Hz in the 17th cycle and ~ 900 Hz in the 18th and last cycle simulated (Fig. 6b).

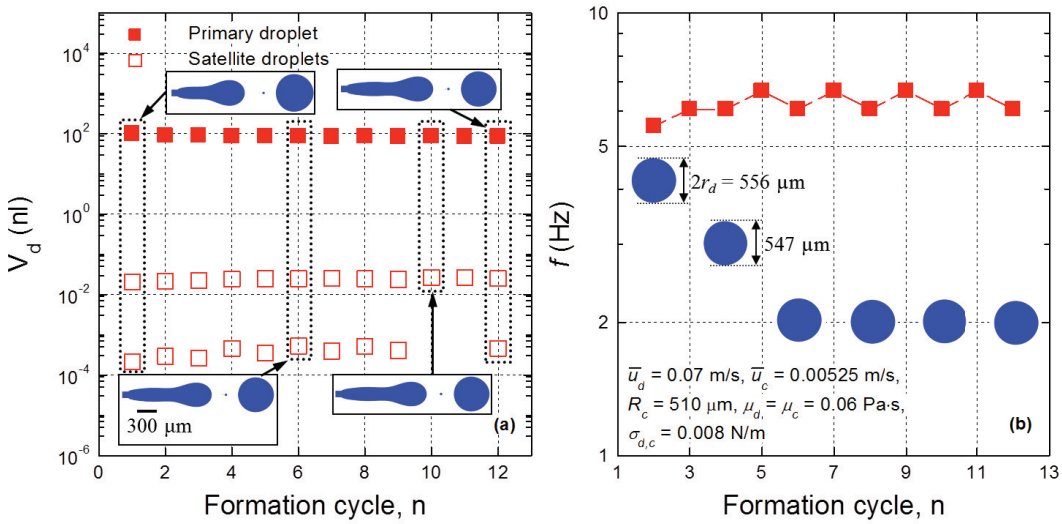

Figure 7. Changes in Disperse Droplet Volume (a) and Formation Frequency (b) with a Widening jet.

While the results presented in Figs. 6a and 6b are for a narrowing jet, those delineated in Figs. 7a and 7b are for a widening jet. The values of the parameters used to generate the results presented in these figures are different from those used for the analysis results presented in Figs. 6a and 6b of a narrowing jet. The radius of the continuous liquid microtube increased to R_c = 510 µm (or R^* = 10.4), the injection velocities of the continuous and disperse liquids decreased to $\overline{u}_c$ = 0.00525 m/s and $\overline{u}_c$ = 0.07 m/s, the dynamic viscosities of both liquids increased to 0.06 Pa·s, and the interfacial tension significantly decreased to $\sigma_{d,c}$.= 0.008 N/m. As for a narrowing jet, the break off of the disperse droplets at the tip of a widening jet is by growing and propagating surface perturbations. The results in Figs. 7a and 7b demonstrate the characteristics of the disperse emulsion produced by a stable widening jet, including the volume and the formation frequency of the primary disperse droplets.

The inserted images in Fig 7a show the formation of a stable widening jet with a larger diameter than that of disperse liquid microtube that increases with distance from the exit of the microtube. Unlike a narrowing jet that takes a few cycles to become fully established, the widening jet is stable from the first cycle (Fig. 7a). The length of the widening jet increases somewhat in early cycles, reaching ~2190 µm by the 5th cycle and remains unchanged thereafter (Fig. 7a).

Unlike a narrowing jet, the primary disperse droplets produced in sequential cycles by a widening jet have much larger and close, but not identical sizes (Fig.7a). This is attributed to the large inventory of disperse liquid in a widening jet, compared to a narrowing jet. Consequently, the formation frequency of disperse droplets by a widening jet is significantly lower than by a narrowing jet (Figs. 6b and 7b).

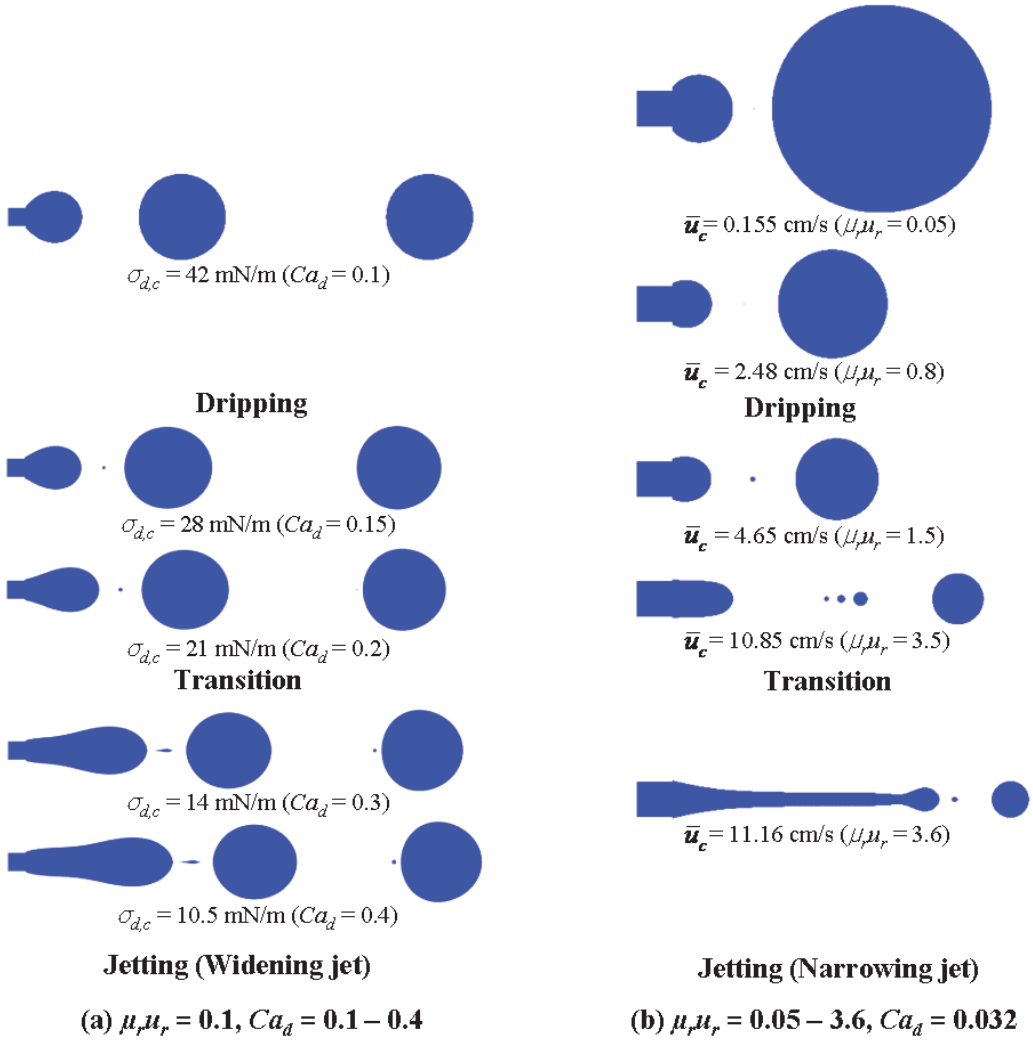

Figure 8. Clips from the Developed Motion Picture Movies of the Formation of Disperse Droplets in the Various Regimes.

As shown in Fig. 7a, the volume of the primary droplet decreases somewhat with the number of cycles, from 98.63 nl (r_d ~286.5 µm) in the 1st cycle to 85.57 nl (r_d ~273.2 µm) in the 5th cycle. After the 5th cycle, the disperse droplets have identical volumes of ~ 85.54 nl (r_d ~273.2 µm). In all simulated cycles of the widening jet, only one or two very small satellite droplets form following the break off the primary droplets. The results in Fig 7b show that the break-off of the primary disperse droplets is associated with little variations in their formation frequency from the mean value (-3.3% to 12.9%). In the present results (Fig. 7b), the frequency of forming disperse droplets by a widening jet is very low, increasing from ~ 6 Hz in the 2nd cycle to ~ 7 Hz in the 5th cycle, and remains constant thereafter.

The results presented in Figs. 4-7 are not inclusive, but only examples of the effect of the various parameters listed in Table 2 on the regime and dynamics of forming disperse droplets using co-flowing immiscible liquids in co-axial microtubes. The parameters in Table 2 are the injection velocities, dynamic viscosities and microtubes diameters of the continuous and disperse liquids and the interfacial tension. Other combinations of these parameters could also be used to establish the different formation regimes of disperse droplets. The present numerical simulations show that the diameter of the forming

disperse droplets by a widening jet is larger than in the dripping regime and by a stable narrowing jet. The polydispersity is absent in the dripping regime, highest in the jetting regime with a narrowing jet, but much less in the transition regime with a widening jet.

Fig. 8 presents select frames of the developed motion picture movies, based on the results of the present numerical simulations. They illustrate visually the different regimes of forming disperse droplets as well as the characteristics of the droplets. Note that the images in Fig. 8a are for different conditions than in Fig. 8b. The conditions for both figures are expressed in term of two dimensionless quantities, namely: the capillary number of the disperse liquid, Ca_d, and the product of the ratios of the dynamic viscosities and injection velocities (or dynamic forces) of the continuous and disperse liquids, $\mu_r \bar{u}_r$. The shift from dripping to transition and from the latter to the jetting regime in Fig. 8a is achieved by decreasing the interfacial tension (or increasing Ca_d), while keeping other base case parameters in Table 2 constant. In Fig. 8b, the shift among the three regimes of forming disperse droplets is accomplished by increasing the injection velocity of the continuous liquid, while keeping all other base case parameters in Table 2 constant. Comparing the images in Fig. 8 indicates that a widening jet form at high Ca_d (lower interfacial tension) (Fig. 8a), while a narrowing jet forms at much higher interfacial tension and injection velocity of the continuous liquid (Fig. 8b).

The following section presents and discusses the results of the parametric analysis, which investigated the effects of the liquids' properties and injection velocities, the interfacial tension, and the radii of the co-axial microtubes on the regimes of forming disperse droplets. The obtained results are used to develop a flow regimes map and determine the conditions as well as develop dimensionless correlations for the boundaries between the various regimes.

4.2 Parametric Analysis

In the present numerical simulations, the injection rate of the disperse liquid is very low ($We_d << 1, Re_d < 1$). Therefore, the dominant forces for the formation of disperse droplets are the dynamic forces of the continuous and disperse liquids and the interfacial tension. A parametric analysis is carried out by changing the various parameters ($\bar{u}_d$, $\bar{u}_c$, μ_d, μ_c, R_d, R_c and $\sigma_{d,c}$) in the ranges listed in Table 2. The results are presented in Fig. 9-12.

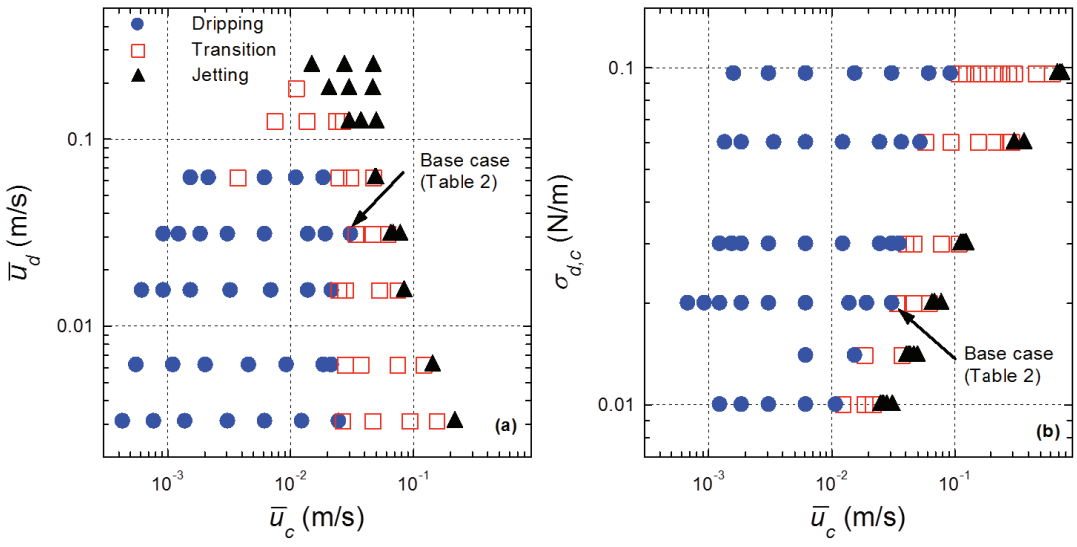

Figure 9. Effects of Injection Velocities of Disperse and Continuous liquids and Interfacial Tension on the Formation of Disperse Droplets in Various Regimes.

Increasing the injection velocity of continuous liquid extends the dripping regime and shifts the formation of disperse droplets from dripping to transition and then to jetting regime (Figs. 9a and 9b). The width of the transition regime increases as the interfacial tension increases, causing the shift to the jetting regime to occur at higher injection velocities of the continuous liquid. In Fig. 9b, increasing the interfacial tension from 0.01 to 0.0961 increases the injection velocity of the continuous liquid to shift from dripping to transition from 0.0124 m/s to 0.124 m/s, and from 0.0248 m/s to 0.682 m/s for shifting from the transition to the jetting regime. Other properties that affect the boundaries between the three regimes of forming disperse droplets are the dynamic viscosities of the liquids. The results of the effects of these properties are given in Figs. 10a and 10b.

The results in Figs. 9a and 9b show the effects of increasing the injection velocities of disperse and continuous liquids and the interfacial tension on the prevailing regime of forming disperse droplets. The results also show the conditions for the boundaries between the three regimes of forming disperse droplets, namely: dripping, transition and jetting. The jetting regime results include both narrowing and widening jets (Fig. 8). Increasing the injection velocity of either the continuous or the disperse liquid extends the dripping regime, and shifts the formation of disperse droplets to the transition, then to the jetting regime (Fig. 9a). In general, increasing the injection velocity of disperse liquid increases the dynamic viscousity and inertial forces for shifting into the various regimes. However, since the inlet Reynolds number of the disperse liquid in the present simulations (Table 2) is less than unity, the viscous force of disperse liquid is more important than its inertia for the formation of droplets in the various regimes.

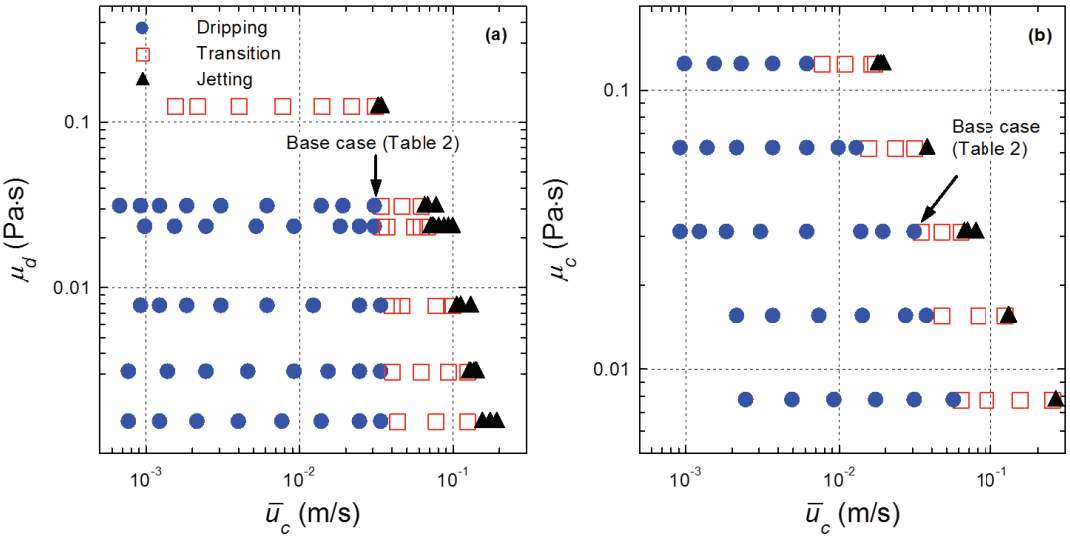

Figure 10. Effects of Disperse and Continuous Liquids Viscosities on the Regimes of Forming Disperse Droplets.

The results presented in Figs. 10a and 10b confirm that increasing the injection velocity of the continuous liquid shifts the formation of disperse droplets from dripping to transition and then to the jetting regime. Figure 10a shows the boundary between the dripping and transition regimes is independent of the dynamic viscosity of the disperse liquid < 0.031 Pa·s and that the shift to the transition regime occurs when the injection velocity of the continuous liquid, $\bar{u}_c$, is ~ 0.031 m/s. Similarly, increasing the dynamic viscosity of the continuous liquid, μ_c, increases the drag exerted on the interface between the co-flowing liquids, decreasing the continuous liquid velocity for shifting from the transition to the jetting regime (Fig. 10b). This figure shows that the dynamic viscosity of the continuous liquid has a pronounced effect on the boundaries among the three regimes of forming disperse droplets.

Increasing the dynamic viscosity of the disperse liquid from 0.0078 to 0.124 Pa·s decreases the injection velocity of the continuous liquid for shifting from the transition to the jetting regime by about 69% (Fig. 10a). The results in Fig. 10b show that increasing the dynamic viscosity of the continuous liquid from 0.0078 to 0.124 Pa·s decreases the injection velocity of the continuous liquid for shifting from the transition to the jetting regime by about 75%. The results of the performed parametric analysis are used in the next section to develop a flow regimes map and dimensionless correlations for the boundaries between the three regimes of forming disperse droplets.

4.3 Flow Regimes Map

The compiled numerical results for the range of parameters listed in Table 2, including R_d = 50 μm and R^* = 6.4 (or R_c = 320 μm), are used to develop the flow regimes map in Fig. 11. This figure plots the capillary number of disperse liquid, Ca_d, versus the ratio of the dynamic forces of the continuous and disperse liquids $\mu_r \bar{u}_r$. The results for the jetting regime are indicated in Fig. 11 by solid triangle symbols and those for the transition regime are indicated by open square symbols. The dripping regime results are represented by solid circle symbols in Fig. 11. This figure also includes the developed dimensionless correlations (Eqs. 7 and 8) for the boundaries separating the dripping, transition and jetting regimes. Figures12a and 12b present the portion of the results in Fig. 11, for $Ca_d \geq 0.09$ and $Ca_d \leq 0.09$, respectively.

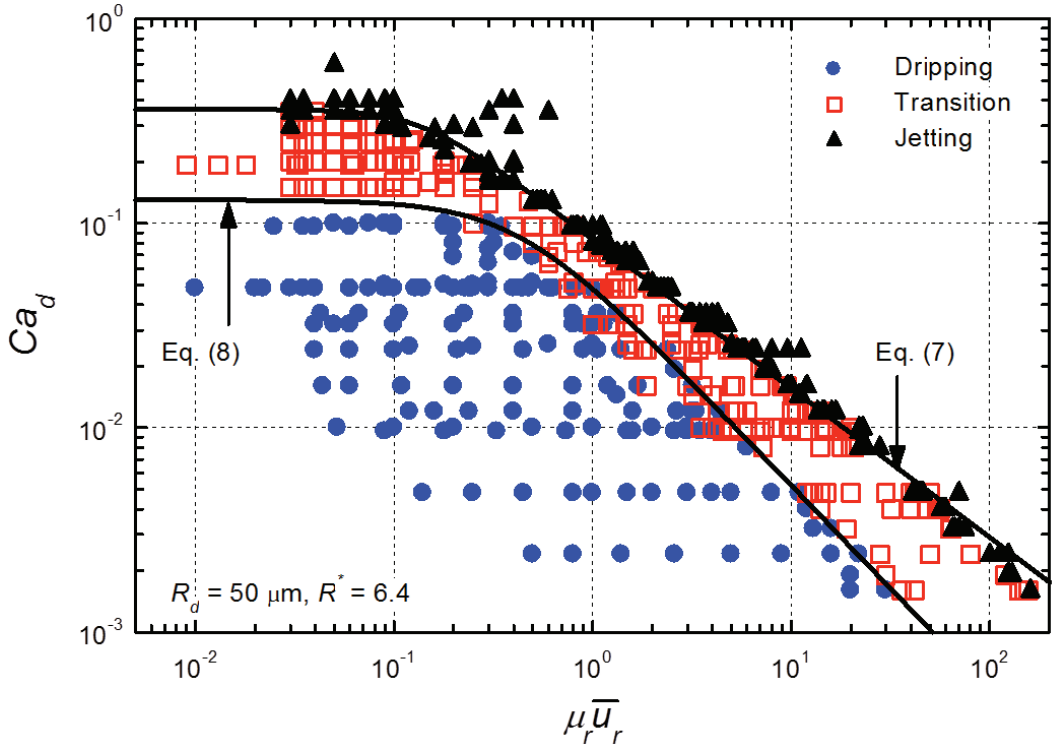

Figure 11. A Flow Regimes Map for the Formation of Disperse Droplets (Dripping, Transition and Jetting)

Increasing the dynamic forces $\mu_r \bar{u}_r$, moves the boundaries between the three regimes of forming disperse droplets to lower values of Ca_d (Figs. 11 and 12). For $Ca_d > 0.1$, the transition regime

dominates, extending to $Ca_d \sim 0.36$. At higher Ca_d values, the jetting regime dominates. The boundary between the transition and jetting regimes, at lower $\mu_r \bar{u}_r$, corresponds to a constant $Ca_d = \sim 0.35$. The values of the capillary number of the disperse liquid for the boundary between the transition and jetting regimes, $Ca_{d,TJ}$ are correlated, in terms of the dimensionless dynamic forces of the continuous and disperse liquids $\mu_r \bar{u}_r$, and the ratio of the disperse and continuous flow microtubes radii, R^*, as:

$$Ca_{d,TJ} = 0.014\, R^{*1.75} \left(1 + 0.01\,(R^{*2}\ \mu_r \bar{u}_r)^{2.7}\right)^{-0.27} \tag{7}$$

The first term on the right hand side of this correlation ($0.014\, R^{*1.75}$) is the highest Ca_d beyond which the boundary between the transient and jetting regimes is independent of $\mu_r \bar{u}_r$ (Fig. 11). Similarly, the developed dimensionless correlation for the boundary between the transition and dripping regimes is given as:

$$Ca_{d,DT} = 0.14 \left(1 + 4.63\, \mu_r \bar{u}_r^{1.74}\right)^{-0.58} \tag{8}$$

In this correlation, the capillary number of the disperse liquid along the boundary is independent of the microtubes radii and solely depends on the ratio of the dynamics forces of the co-flowing liquids.

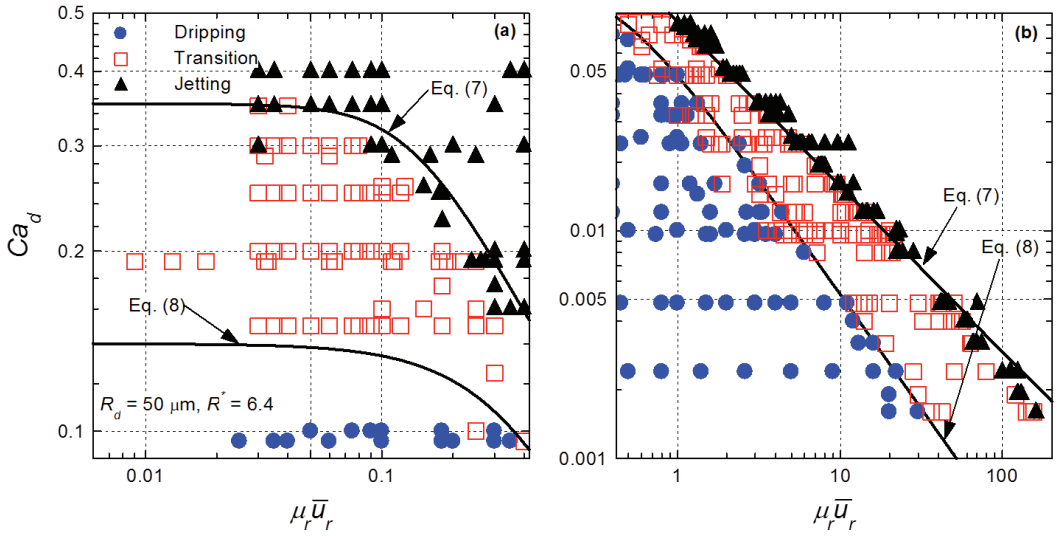

Figure 12. Comparisons of Developed Dimensionless Flow Regimes Map, at Low and High Dynamics Force Ratios, with Numerical Results.

Figures 11 and 12 show good agreement between the numerical calculations and the developed dimensionless correlations for the flow regimes boundaries, Eqs. 7 and 8. The complete flow regimes map in Fig. 11 incorporates a total of 574 data points, including 167 in the dripping regime, 237 in the transition regime and 170 in the jetting regime. The boundary between the transition and jetting regimes is independent of the ratio of the dynamic forces $\mu_r \bar{u}_r$, when $Ca_d > 0.36$ (Fig. 12a). At such capillary numbers, the jetting regime is dominated by widening jets (Fig. 8a). For $\mu_r \bar{u}_r < 0.03$, disperse liquid capillary number along the boundary between the dripping and transition regimes is constant and equals to ~0.14. When $Ca_d < 0.35$, increasing the ratio of the dynamic forces $\mu_r \bar{u}_r$, decreases the corresponding

values of Ca_d along the boundary between the transition and jetting regimes (Fig. 12b). For lower capillary numbers corresponding to $\mu_r \bar{u}_r > 0.4$ (Fig. 12b), the width of the transition regime slightly increases with decreasing Ca_d, whereas the jetting regime becomes dominated by narrowing jets (Fig. 8b).

The results in Figs. 11 and 12 and the developed dimensionless correlations (Equations (7) and (8)) show that the common boundaries between dripping, transition and jetting regimes strongly depend on both Ca_d and $\mu_r \bar{u}_r$. They demonstrate the good agreement between the present numerical results and the developed correlations for the boundaries between the flow regimes (Eqs. (7) and (8)) and the soundness of the developed flow regimes map (Fig. 11).

The results in Figs. 11 and 12 also confirm that the dimensionless quantities, Ca_d, and $\mu_r \bar{u}_r$ are proper choices for constructing the flow regimes map. These dimensionless parameters do not include the ratio of the co-axial microtubes radii, which is included in Eq. (7) and omitted from Eq. (8). The boundary between the transition and jetting regimes depends on the ratio of the microtubes radii, R^* (Eq. (7)), while that between dripping and transition regimes is independent of R^* (Eq. (8)). The effect of R^* on the boundary between the transition and jetting regimes is investigated and the results are presented and discusses next.

4.4 Effect of Microtubes Radii

The numerical results delineated in Figs. 13a and 13b are for the base case parameters in Table 2, but different radii of the continuous liquid microtube, R_c and two radii of disperse liquid microtube, R_d. Figure 13b shows that the boundary between the transition and jetting regimes is independent of the radius of the disperse liquid microtube, R_d. However, it strongly depends on that of the continuous liquid microtube, R_c, or the radii ratio, R^*. Increasing R^*, moves the boundary between transition and jetting outward to higher Ca_d and dynamics forces ratio, $\mu_r \bar{u}_r$ (Fig. 13a). There is a value of Ca_d, beyond which that boundary becomes independent of $\mu_r \bar{u}_r$; and it increases with increasing R^*. This value is ~ 0.1 at R^*= 3.2, and ~ 0.8 at R^* = 10.2. The shift in the boundary between the transition and jetting regimes with increasing R^* is much smaller at higher $\mu_r \bar{u}_r$ (> 0.3 for R^*= 3.2 and > 0.03 for R^*= 10.2).

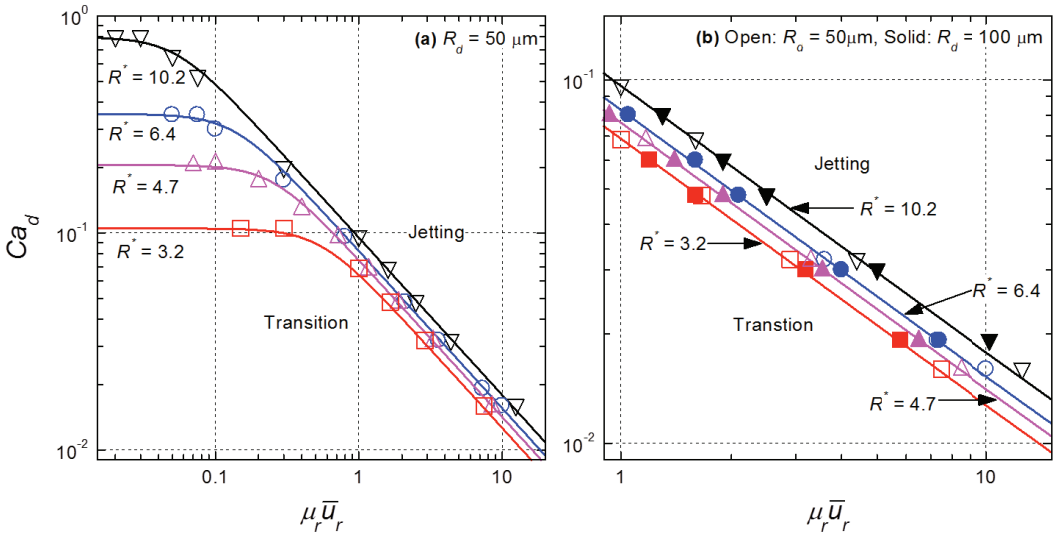

Figure 13. Effect of Microtubes Radii on the Boundary Between Transition and Jetting Regimes for Forming Disperse Droplets.

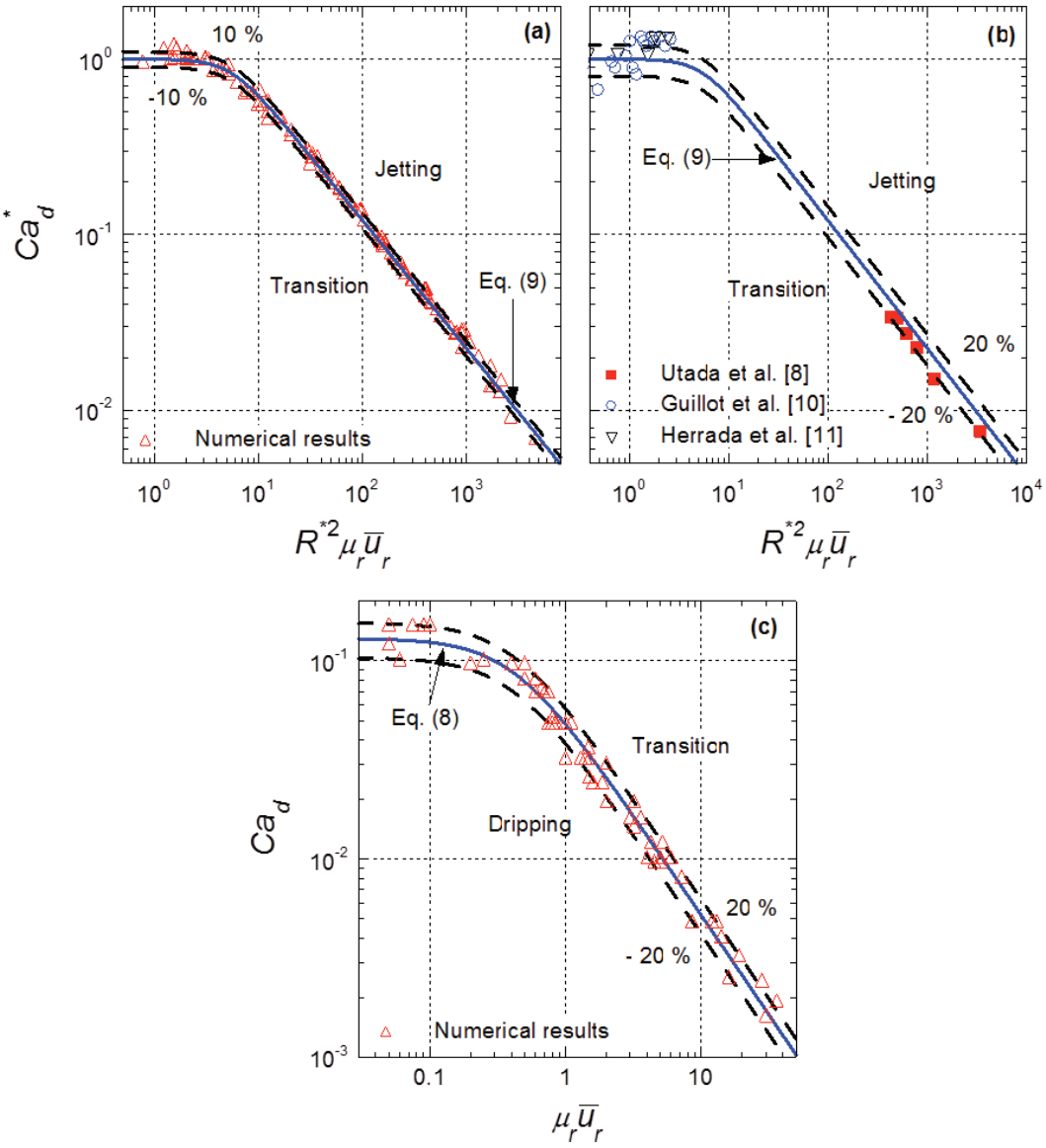

Figure 14. Comparisons of Present Correlations for Flow Regimes Boundaries with Numerical Results (a) & (c) and Experimental Measurements (b).

Increasing R^*, expands the transition regime toward jetting. For example, increasing R^* from 3.2 to 10.2 increases the capillary number of the disperse liquid for the boundary between the transition and jetting regimes by about 8 times. Similarly, when Ca_d is less than its value for the boundary between transition and jetting, the ratio of the dynamic forces $\mu_r\bar{u}_r$, along that boundary increases with increasing R^*. At $Ca_d = 0.016$, increasing R^* from 3.2 to 10.2 changes the value of $\mu_r\bar{u}_r$ to shift from transition to jetting from 7.5 to 12.5 (Fig. 13b). Figure 13b also shows that for same R^*, the radius of disperse liquid microtube, R_d, (50 μm and 100 μm), does not affect the boundary between the transition and jetting regimes. However, this boundary strongly depends on R^* or the radius of the continuous liquid, R_c.

The effect of R^* on the boundary between the transition and jetting regimes is indicated by the first term of the dimensionless correlation in Equation (7). This term ($0.014\ R^{*1.75}$) is the value of Ca_d,

beyond which the boundary between the transient and jetting regimes is independent of $\mu_r \bar{u}_r$ (Figs. 11 and 13a). When normalized relative to this term, Equation (7) is simply rewritten as:

$$Ca^*_{d,TJ} = \left\{1 + 0.01\left(R^{*2}\mu_r \bar{u}_r\right)^{2.7}\right\}^{-0.27} \tag{9}$$

In this equation, $Ca^*_{d,TJ}$, the normalized disperse liquid capillary number = Ca_d/ (0.014 R^*).

Figure 14a compares the present numerical calculations, for the different ranges of the parameters in Table 2, with the developed dimensionless correlation in Eq. (9) for the boundary between transition and jetting. Figure 14b compares this correlation with the reported experimental results for different immiscible liquids [8,10,11]. As Figs. 14a and 14b show, Eq. (9) is in good agreement with both the present numerical and the reported experimental results, to within ± 10% and ± 20%, respectively. Figure 14c compares the present numerical results for R^* = 3.2, 4.7, 6.4, 10.2, 12.2 with the developed dimensionless correlation for the boundary between dripping and transition (Eq. (8)). The numerical results in Fig. 14c agree with Equation (8) to within ±20%.

Unlike the boundary between the transition and jetting regimes (Figs. 14a and 14b), that between the dripping and transition regimes is independent of R^* (Fig. 14c and Eq. (8)). This is because the breakup of the disperse droplets in the dripping regime depends on the dynamics forces of the co-flowing liquids and the interfacial tension. This continues to be the case in the transition regime, where the length of disperse liquid thread (Fig. 2) is relatively short to affect the primary droplets' break off. On the other hand, in the jetting regime the radius of the continuous liquid microtube, R_c, affects the length, radius and type of the forming disperse liquid jets, and hence the disperse droplets' formation.

4.5 Validation of Present Correlations

To further examine the fidelity and accuracy of the present numerical simulations, the correlations in Equations (8) and (9) are compared in Figs. 15a and 15b with the experimental data of Cramer et al. [4], Gu et al. [7], Utada et al. [8], Guillot et al [10] and Herrada et al [11]. The experimental data of Cramer et al. is for disperse aqueous solution of κ-Carrageeenan and sunflower oil in co-axial microtubes with R^* = 44.44. The experimental data of Gu et al. [7] is for disperse aqueous solution of sodium alginate and salad oil in co-axial microtubes with different radii ratios, R^* = 2.5-6.7. The experimental results of Utada et al. [8] are for disperse ionized water and PDMS (Polydimethylsiloxane) oil in co-axial microtubes with R^* = 10. The experimental data of Guillot et al. and Herrada et al. is for disperse aqueous solution of glycerine and silicone oil, with and without surfactant (Sodium Dodecyl Sulfate), in co-axial microtubes with R^* = 13.8.

Figure 15a shows a spread in the reported experimental data by the different investigators in the dripping regime. Nonetheless, the developed dimensionless correlation in Equation (8), for the boundary between dripping and transition, is consistent with the trend displayed by the experimental data. Similarly, the correlation in Eq. (9) for the boundary between the transition and jetting regimes is consistent with the experimental data in Fig. 15b. The spread in the experimental data in Figs. 15a and 15b partially stems from the fact that researchers had focused in their experiments on the jetting regime, considering transition and dripping a single regime. This is shown in the present analysis not to be the case.

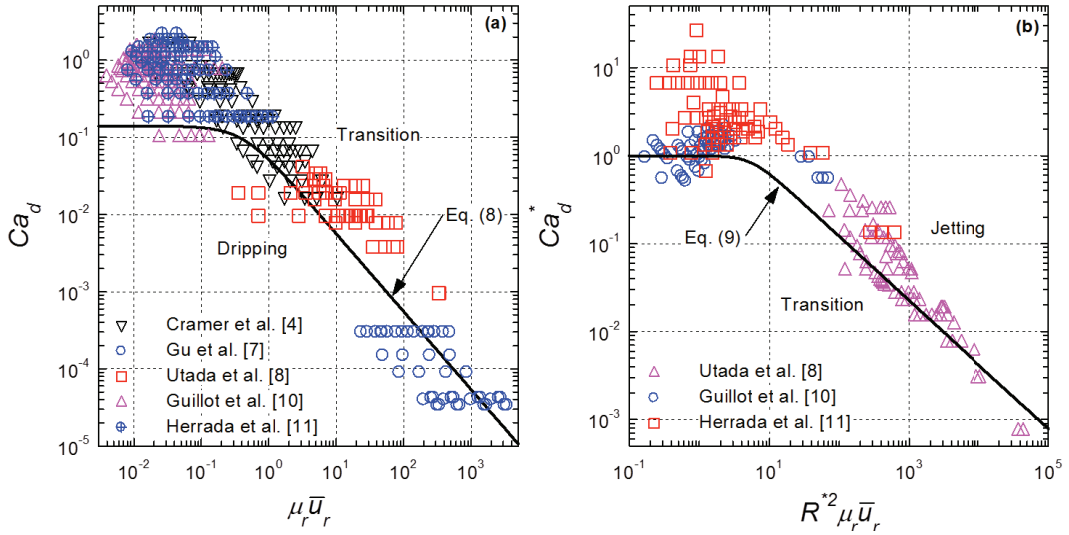

Figure 15. Comparisons of Present Correlations for the Boundaries between Dripping and Transition (a) and between Transition and Jetting (b), with Experimental Data.

The reported regimes map by Utata et al. [8], based on their experimental results, identifies the boundary between transition and jetting (Fig. 16). Their results are compared with the present correlations (Eqs. (7 and 8)) and the results of linear instability analysis by Herrada et al. [11]. Utata et al.[8] did not explicitly acknowledge the transition regime, they considered it a part of the dripping regime.

The present correlation (Eq. (7)) for the boundary between transition and jetting agrees well with the experimental data of Utata et al. [8]. The linear instability analysis predictions of that boundary are consistently lower than the experimental results, and higher than the present correlation (Eq. (8)) for the boundary between dripping and transition. Herrads et al. [11] results of linear instability analysis, which neglects the inertia of the co-flowing liquids, are lower than the present correlation (Eq. (7)) for $Ca_d < 0.1$, but higher at higher values of Ca_d.

Figure 16 shows that at high dynamics force ratios $\mu_r \bar{u}_r > 1.0$, the predictions of the instability analysis of the boundary between transition and jetting are lower than both the present correlations and the experimental data of Utata et al. [8]. However, the difference decreases as the dynamics force ratio decreases. For $\mu_r \bar{u}_r < 1.0$, the instability analysis predicts higher Ca_d values than the present correlation (Eq. (7)) for the boundary between transition and jetting.

The good agreement of the experimental results of Utata et al. [8] in Fig. 16 with Equation (7) for the boundary between transition and jetting is noteworthy. It confirms the fidelity of the present calculations, the solution methodology and the constituent equations used in the numerical simulations. In addition, this agreement confirms the appropriate choices of the dimensionless parameters in Equations (7) and (8) for the boundaries between dripping, transition and jetting regimes.

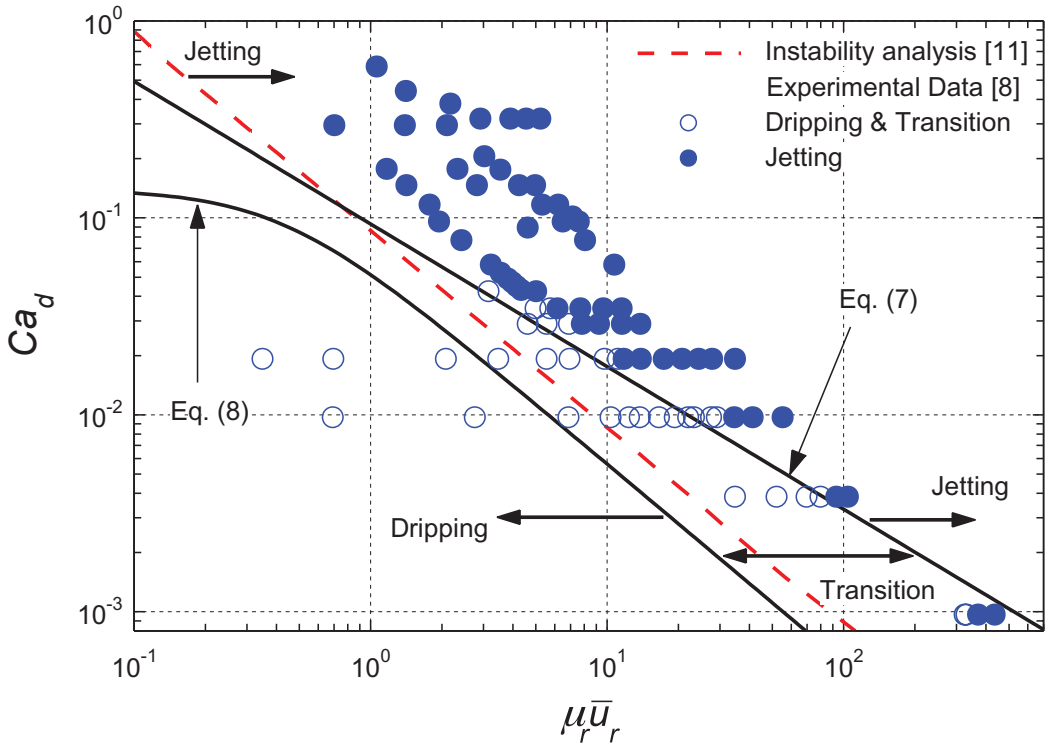

Figure 16. Comparisons of Developed Correlations of the Boundaries between Dripping, Transition and Jetting Regimes, with Results of Instability Analysis [11] and Experimental Data [8].

5. SUMMARY AND CONCLUSION

This paper numerically simulates co-flowing immiscible liquids in co-axial microtubes for forming disperse droplets and investigates the effects of the injection velocities, inner microtubes diameters and physical properties of the liquids and the interfacial tension on the characteristics and the regimes of forming disperse droplets. The results are used to develop dimensionless correlations for the boundaries between the dripping, transition and jetting regimes of forming disperse droplets.

The numerical solution simultaneously solves the transient Navier-Stockes equations of the co-flowing liquids and the advection equation for the evolving interface, in conjunction with the momentum jump condition. The location and shape of the evolving interface between the continuous and disperse co-flowing liquids (Figs. 3) are determined using the Level Set method [5,27,28].The present numerical simulations employed the commercial software package of COMSOL 4.0a.

The numerical mesh grid in the numerical computation domain for the present simulations comprises quadrilateral mesh elements of a uniform size (5 x 5 μm). The total number of the mesh elements in the domain increases from 9,560 to 60,650, commensurate with radius of the continuous liquid (Table 2). Using a finer numerical grid, insignificantly changes the results, but increases computation time. The overall mass balance in the numerical simulations is satisfied with < 6% error. Such an error is caused by the difficulty accounting for the total mass of all the tiny satellite droplets forming in the simulations.

The length of the computation domain provided enough distance, from the tip of disperse liquid capillary, to obverse at least 3-5 formation cycles of the primary disperse droplets, including the first one. The numerical simulations continued for up to 18 cycles of forming disperse droplets, depending on the prevailing regime (dripping, transition or jetting). The results are used to produce motion picture movies for characterizing the growth dynamics and the break off of the disperse droplets in dripping, transition and jetting regimes. The results are also used to developed a flow regimes map and correlations, expressed in terms of the dimensionless quantities: $Ca_{d,DT}$, $Ca_{d,TJ}$, $\mu_r\bar{u}_r$, $R^*\mu_r\bar{u}_r$ and R^*, for predicting the boundaries between the dripping, transition and jetting regimes.

The developed correlations for these boundaries are in good agreement with the present numerical results to within $\pm$10% and within $\pm$20% of the reported experimental measurements using different co-flowing liquids. These include ionized water and PDMS (Polydimethylsiloxane) oil with $R^* = 10$, and aqueous solutions of glycerine into silicone oil flow, with and without surfactant (Sodium Dodecyl Sulfate) with $R^* = 13.8$. These agreements validate the present numerical results and confirm the fidelity of the developed flow regimes map. This map and the developed correlations for the boundaries between the dripping, transition and jetting regimes are useful and valuable tools for industrial and medical applications of micro-emulsions and their production on a large scale and to the design of prototypes of micro-systems.

NOMENCLATURE

Ca_c	Capillary number of continuous liquid, $\mu_c\bar{u}_c/\sigma_{d,c}$
Ca_d	Capillary number of disperse liquid, $\mu_d\bar{u}_d/\sigma_{d,c}$
$Ca_{d,DT}$	Capillary number for dripping-transition boundary.
$Ca_{d,TJ}$	Capillary number for transition-jetting boundary.
$Ca^*_{d,TJ}$	Normalized Capillary number for transition-jetting boundary
f^*	Dimensionless frequency of forming disperse droplets
g	Acceleration of gravity (m/s^2)
L	Microtube length (μm)
p	Pressure (Pa)
Q	Liquid flow rate (μl/s)
R	Microtube radius (μm)
$R_{d,o}$	Outer radius of inner microtube (μm)
R^*	Ratio of microtubes radii, R_c/R_d
r	Radial distance (μm)
r_d	Radius of disperse droplet (μm)
r^*_d	Dimensionless radius of disperse droplet
u	Flow velocity (m/s)
$\bar{u}$	Average injection velocity (m/s)
$\bar{u}_r$	Average injection velocities ratio, $\bar{u}_c/\bar{u}_d$
Re_c	Injection Reynolds number of continuous liquid, $2(R_c - R_{d,o})\rho_c\bar{u}_c/\mu_c$
Re_d	Injection Reynolds number of disperse liquid,
t	Time (s)
V_d	Disperse droplet volume (nl)
We_d	Weber number of disperse flow, $2R_d\rho_d\bar{u}_d^2/\sigma_{d,c}$
z	Axial distance (μm)

Greeks

ϕ	Distance function of interface (mm)
κ	Interface curvature (m^{-1})
μ	Liquid viscosity (Pa·s)
μ_r	Liquid viscosity ratio, μ_d/μ_c
ρ	Liquid density (kg/m^3)

$\sigma_{d,c}$	Interfacial tension (N/m)
τ	Shear stress, (Pa)

Subscripts

c	Continuous
d	Disperse
int	Interface
n	Liquid identifier, (continuous or disperse)

ACKNOWLEDGMENTS

The University of New Mexico's Institute for Space and Nuclear Power Studies funded this research.

REFERENCES

[1] Link, D. R., G.-Mongrain, E., Duri, A., Sarrazin, F., Cheng, Z., Cristobal, G., Marquez, M., and Weitz, D. A., Electric Control of Droplets in Microfluidic Devices, *Angew. Chem*., 2006, 118, 2618-2622.

[2] Morimoto, Y., Tan, W.-H., and Takeuchi, S., Three-dimensional Axisymmetric Flow-focusing Device Using Stereolithography, *Biomed. Microdevices*, 2009, 11, 369-377.

[3] Cordero, M. L., Gallaire, F., and Baroud, C. N., Quantitative Analysis of the Dripping and Jetting Regimes in Co-flowing Capillary Jets, *Phys. Fluids*, 2011, 23(9), paper no. 094111.

[4] Cramer, C., Fischer, P., and Windhab, E. J., Drop Formation in a Co-flowing Ambient Fluid, *Chem. Eng. Sci*., 2004, 59(15), 3045–3058.

[5] Yang, I. H., and El-Genk, M. S., Emulsion Formation in Dripping Regime of Co-flowing Immiscible Liquids in Co-axial Micro-tubes, *Micro-Nono Scale Transport*, 2011, 2(1), 57 – 83.

[6] Hua, J., Zhang, B., and Lou, J., Numerical Simulation of Microdroplet Formation in Coflowing Immiscible Liquids, *AIChE Journal*, 2007, 53(10), 2534-2547.

[7] Gu, Y., Kojima, H., and Miki, N., Theoretical Analysis of 3D Emulsion Droplet Generation by a Device Using Coaxial Glass Tubes, Sens. *Actuators A: Phys*., 2011, 169(2), 326–332.

[8] Utada, A. S., Fernandez-Nieves, A., Stone, H. A., and Weitz, D. A., Dripping to Jetting Transitions in Coflowing Liquid Streams, *Phys. Rev. Lett*., 2007, 99(9), paper no. 094502.

[9] Castro-Hernandez, E., Gundabala, V., Fernandez-Nieves, A., and Gordillo, J. M., Scaling the Drop Size in Coflow Experiments, *New J. Phys*., 2009, 11(7), paper no. 075021.

[10] Guillot, P., Colin, A., Utada, A. S., and Ajdari, A., Stability of a Jet in Confined Pressure-driven Biphasic Flows at Low Reynolds Numbers, *Phys. Rev. Lett*., 2007, 99(10), paper no. 104502.

[11] Herrada, M. A., and Ganan-Calvo, A. M., Spatiotemporal Instability of a Confined Capillary Jet, *Phys. Rev. E*, 2008, 78, paper no. 046312.

[12] Colin, T., and Tancogne, S., Stability of Bifluid Jets in Microchannels, *Eur. J. Mech. B-Fluids*, 2011, 30, 409-420.

[13] Zhang, X., and Basaran, O. A., An Experimental Study of Dynamics of Drop Formation, *Phys. Fluids*, 1995, 7(6), 1184-1203.

[14] Homma, S., Koga, J., Matsumoto, S., Song, M., and Tryggvason, G., Breakup Mode of an Axisymmetric Liquid Jet Injected into Another Immiscible Liquid, *Chem. Eng. Sci*., 2006, 3(3), 341-346.

[15] Jin, F., Gupta, N. R., and Stebe, K. J., The Detachment of a Viscous Drop in a Viscous Solution in the Presence of a Soluble Surfactant, *Phys. Fluids*, 2006, 18(2), paper no. 022103.

[16] Rayleigh, L., On the Instability of Jets, *Proc. London Math. Soc*., 1879, 10, 4- 13.

[17] Rayleigh, L., On the Instability of a Cylinder of Viscous Liquid under Capillary Force, *Phil. Mag*., 1892, 34, 145-154.

[18] Tomotika, S., On the Instability of a Cylindrical Thread of a Viscous Liquid Surrounded by Another Viscous Fluid, *Proc. R. Soc. Lond. A*, 1935, 150(870), 322-327.

[19] Plateau, J., *Experimental and Theoretical Statics of Liquid Vol. 2*, Gauther-Villars, Paris, 1873, Chap. 11.

[20] Taylor, G. I., The Formation of Emulsions in Definable Fields of Flow, *Proc. R. Soc. Lond. A*, 1934, 146(858), 501-523.

[21] O'Donnel, B., Chen, J. N., and Lin, S. P., Transition from Convective to Absolute Instability in a Liquid Jet, *Phys. Fluids*, 2001, 13(9), 2732-2734.

[22] Leib, S. J., and Goldstein, M. E., The Generation of Capillary Instabilities on a Liquid Jet, *J. Fluid. Mech.*, 1986, 168, 479-500.

[23] Leib, S. J., and Goldstein, M. E., Convective and Absolute Instability of a Viscous Liquid Jet, *Phys. Fluids*, 1986, 29(4), 952-954.

[24] Huerre, P., and Monkewitz, P. A., Local and Global Instabilities in Spatially Developing Flows, *Annu. Rev. Flud. Mech.*, 1990, 22, 473-537.

[25] Saarloos, W. V., Front Propagation into Unstable State: Marginal Stability as a Dynamical Mechanism for Velocity Selection, *Phys, Rev. A*, 1988, 37(1), 211-229.

[26] Saarloos, W. V., Front Propagation into Unstable States, *Phys. Rep.*, 2003, 386, 29-229.

[27] Olsson, E., Kreiss, G., and Zahedi, S., A Conservative Level Set Method for Two Phase Flow II, *J. Computational Phys.*, 2007, 225(1), 785-807.

[28] *Comsol CFD user's guide*, Comsol AB., Stockholm, 2010, 155-272.

[29] El-Genk, M. S., Yang, I.-H., Friction Number and Viscous Dissipation Heating for Laminar Flows of Water in Microtubes, *J. Heat Transfer*, 2008, 130(8), paper no. 082405.